Journal of Experimental Nanoscience
Publication details, including instructions for authors and subscription information:
http://www.informaworld.com/smpp/title~content=t716100757

Facile mixed-solvent-thermal synthesis and characterisation of LaF_3 : Eu^{3+}/Tb^{3+} monodisperse nanoparticles

Bing Yan[a]; Jianhua Wu[a]
[a] Department of Chemistry, Tongji University, Shanghai, China

To cite this Article Yan, Bing and Wu, Jianhua(2009) 'Facile mixed-solvent-thermal synthesis and characterisation of LaF_3 : Eu^{3+}/Tb^{3+} monodisperse nanoparticles', Journal of Experimental Nanoscience, 4: 1, 1 — 7
To link to this Article: DOI: 10.1080/17458080802688435
URL: http://dx.doi.org/10.1080/17458080802688435

Journal of Experimental Nanoscience
Vol. 4, No. 1, March 2009, 1–7

Taylor & Francis
Taylor & Francis Group

Facile mixed-solvent-thermal synthesis and characterisation of $LaF_3:Eu^{3+}/Tb^{3+}$ monodisperse nanoparticles

Bing Yan* and Jianhua Wu

Department of Chemistry, Tongji University, Shanghai, China

(*Received 17 November 2008; final version received 14 December 2008*)

LaF_3 : 10% Eu^{3+}/Tb^{3+} monodisperse nanoparticles have been synthesised by a novel mixed-solvent-thermal technology (*N*,*N*-dimethyl-formamide (DMF), diethylene glycol (DEG)). When the volume ratio of mixed-solvents (DMF : DEG) is 6 : 12, LaF_3 : 10% Eu^{3+}/Tb^{3+} nanoparticles show a pure hexagonal phase structure with space group of *P*63/*mcm*. Both the X-ray diffraction pattern and the transmission electron microscope image present a uniform microstructure with good dispersibility, and its particle size is around 10 nm. The characteristic green emissions of Tb^{3+} originate from $^5D_4 \rightarrow {}^7F_J$ ($J = 6, 5, 4, 3$) transitions and the red emissions of Eu^{3+} from $^5D_0 \rightarrow {}^7F_J$ ($J = 1, 2, 3, 4$) transitions can be observed. The dominant peaks are situated at 543 and 590 nm, respectively.

Keywords: monodisperse nanocrystal; microstructure; luminescence; mixed-solvent-thermal synthesis

1. Introduction

Luminescent nanomaterials have attracted considerable attention for their various potential applications such as optical devices [1,2], chemical or biological labels and probes [3,4], low-threshold lasers [5], and so on. The research emphasis on nanostructure materials development has gradually shifted from the preparation of the materials to the relationship between the nanostructure and the size-dependent properties. Therefore, the formation of monodisperse nanocrystals with controlled size and shape has recently become a central topic in the field of materials chemistry [6–10]. Development in the field not only means a challenge for synthetic chemistry, but also for optoelectronics [11,12], biomedical sensors [13,14], crystallisation [15] and biomineralisation [16–18], etc.

Solution-based wet chemical processes provide attractive routes to synthesise rare earth fluoride with nanostructure. Many of them are based on the precipitation of the Ce^{3+} ion in all kinds of solution to generate CeF_3 and the subsequent separation. For example, all kinds of microemulsion systems or reverse microemulsion systems are utilised to synthesise lanthanide fluorides nanometre material [19–24]. Yttrium fluoride nanoparticles with various crystallinity, shape, and particle size have been prepared by precipitation in reverse

*Corresponding author. Email: byan@tongji.edu.cn

ISSN 1745–8080 print/ISSN 1745–8099 online

DOI: 10.1080/17458080802688435
http://www.informaworld.com

microemulsions of water in cyclohexane solution stabilised with polyoxyethylene isooctylphenyl [25]. In this system, the mixtures of monodisperse regular hexagonal and triangular single nanocrystals can be observed. This method exploits two useful properties of reverse microemulsion, the capacity to dissolve reactants in the water core and the constant exchange of the aqueous phase among micelles, but unfortunately the intricate operation hinders the application of the method in large-scale production.

Because of the excellent coordination ability of *N*,*N*-dimethyl-formamide (DMF) to rare earth ions, the interaction between DMF and rare earth ions may be expected to change the precipitation process of rare earth compounds. In this article, we adopt an effective way to synthesise shape-controlled and mondisperse $LaF_3:10\%$ Eu^{3+}/Tb^{3+} nanocrystals under mild conditions. The mixed solvents of DMF and diethylene glycol (DEG) are adopted to prepare $LaF_3:10\%$ Eu^{3+}/Tb^{3+} nanoparticles. The precipitation reaction process is induced by the heat treatment at 120°C, which is much lower than the temperature of polyol process.

2. Experimental section

2.1. *Synthesis of luminescent $LaF_3:Eu^{3+}/Tb^{3+}$ nanoparticles*

In a typical procedure, 1.8 mmol of $La(NO_3)_3 \cdot 6H_2O$, and 0.2 mmol of $RE(NO_3)_3 \cdot 6H_2O$ (RE = Eu, Tb) were dissolved in 6 mL DMF solvent, and 6 mmol NH_4F was dipped in 12 mL DEG. Then the above DMF solution was added into the DEG solution with magnetic stirring. A gel-like precipitate formed immediately. After continuous stirring for about 15 min, the precipitate was dissolved again and the mixed suspension became a clear solution. The homogeneous solution was transferred to a Teflonlined stainless-steel container, sealed and maintained at 120°C for 24 h. Finally, it was allowed to cool slowly to room temperature. The white products were collected by centrifugal separation, washed several times with distilled water and absolute ethanol, and finally dried at 60°C for 4 h.

2.2. *Physical characterisation*

Fourier transform infrared (FTIR) spectra were measured within the 4000–400 cm^{-1} region on an (Nicolet model 5SXC) infrared spectrophotometer with the KBr pellet technique. X-ray diffraction (XRD) was recorded on a Bruck D8-Advance X-ray diffractometer with monochromatised Cu-Kα radiation ($\lambda = 1.54056$ Å). The micromorphology was performed with a JEM1230 (JEOL, Japan) transmission electron microscope (TEM) at an accelerating voltage of 120 kV, and a JEM2010 high-resolution TEM, at 200 kV. The excitation and emission spectra were determined on a RF-5301 spectrophotometer whose excitation and emission slits width were both 3 nm.

3. Results and discussion

Figure 1 shows the selected XRD pattern of $LaF_3:Eu^{3+}$ nanoparticles by the mixed solvents (volume ratio DMF : DEG = 6 : 12) – thermal synthesis. These samples are in good agreement with hexagonal phase structure, which crystallises in *P*3*c*l space group

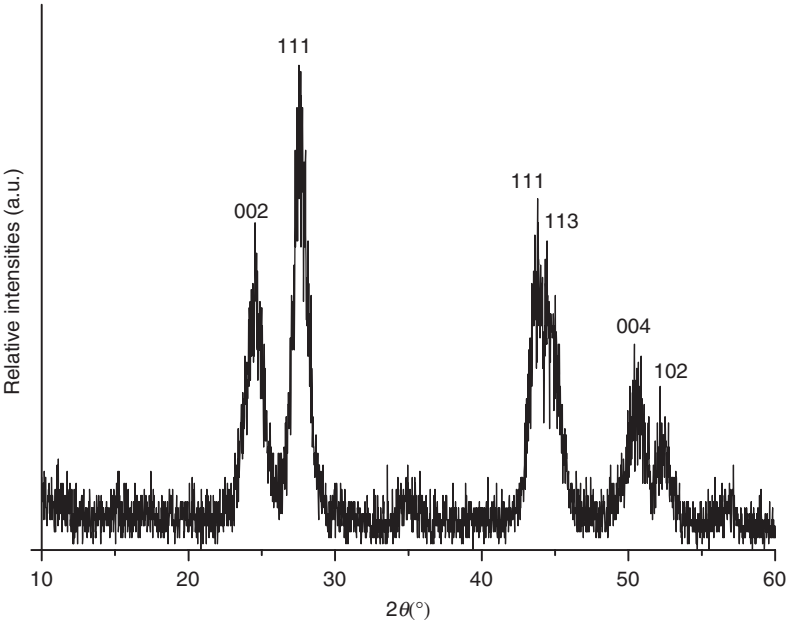

Figure 1. The XRD pattern of a serial of $LaF_3:10\%Eu^{3+}$ nanoparticles with volume ratio 6 : 12 of DMF/DEG.

known from the bulk LaF_3 crystal (JCPDS database No. 82-0684). Eu^{3+} replaces the position of La^{3+} in the LaF_3 host and cannot change the lattice structure. Besides, all peaks broaden obviously owing to the small size of the particles. The crystallite size can be estimated from the Scherrer equation, $D = 0.941\lambda/\beta\cos\theta$, where D is the average grain size, λ is the X-ray wavelength (0.15405 nm), and θ and β are the diffraction angle and full-width at half-maximum (FWHM) of observed peak, respectively. The strongest and independent peak (111) at $2\theta = 27.8^\circ$ is used to calculate the grain size of the nanocrystals and the calculated size of the nanoparticles is around 9.0 nm, which delegates the dimension in the normal direction of (111) plane.

Figure 2 shows the selected TEM picture $LaF_3:10\%Eu^{3+}$ nanoparticle, which shows the homogenerous and uniform microstructure. The aggregation of LaF_3 particles has been hindered and the arrangement of products is close to the monodispersibility. The particle size can be estimated at around 10 nm, which is in agreement with the determination from XRD. Owing to the high-boiling point, high viscosity and reduction properties, the polyol process is an effective way to synthesise very small and metastable particles at a relatively high temperature, but it is not a better process for shape-controlled synthesis.

The excitation spectrum of $LaF_3:Eu^{3+}$ is shown in Figure 3(a) with the emission wavelength of 613 nm. Some characteristic excitation bands can be observed. The apparent broad band is in the near ultraviolet region of 200–350 nm with a maximum excitation of 285 nm, which is ascribed to be the charge transfer band (CTB) between F^- to central Eu^{3+}. The wide strong excitation band of CTS is favourable for the energy transfer and luminescence of Eu^{3+}. The nano effect on the broadening of the CTB of F^- and Eu^{3+} can

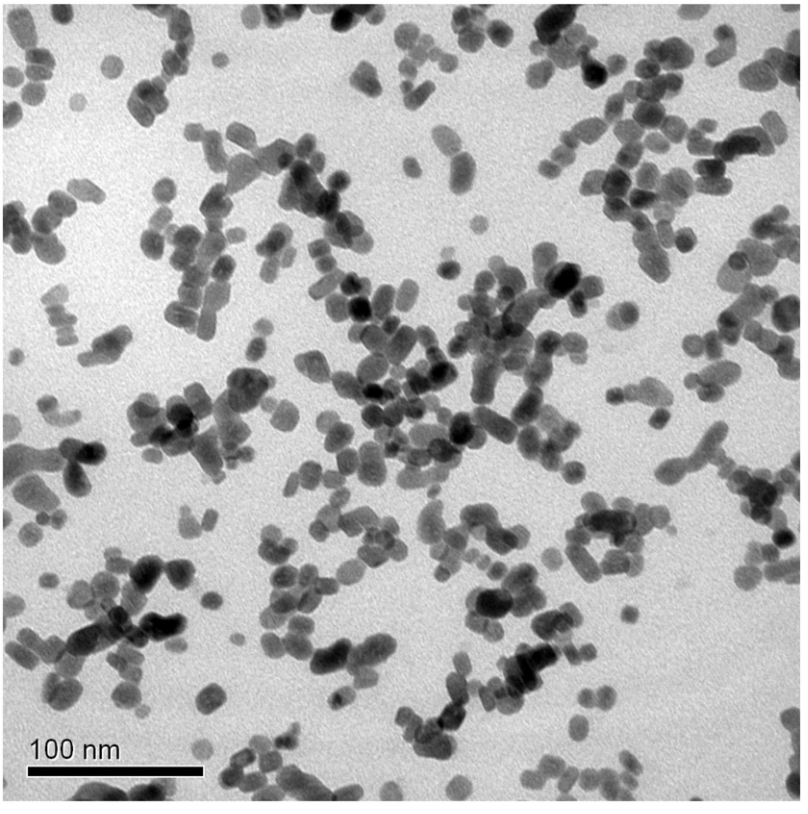

Figure 2. Selected TEM image of $LaF_3:10\%Eu^{3+}$ synthesised with volume ratio 6:12 of DMF/DEG.

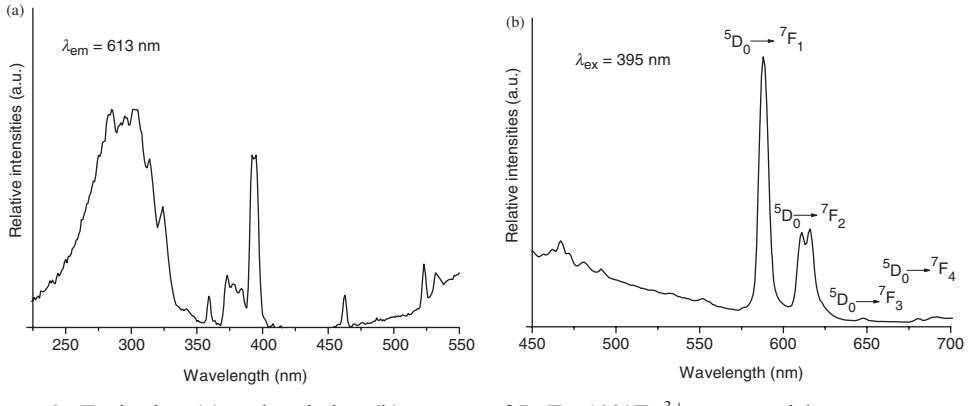

Figure 3. Excitation (a) and emission (b) spectra of $LaF_3:10\%Eu^{3+}$ nanoparticles.

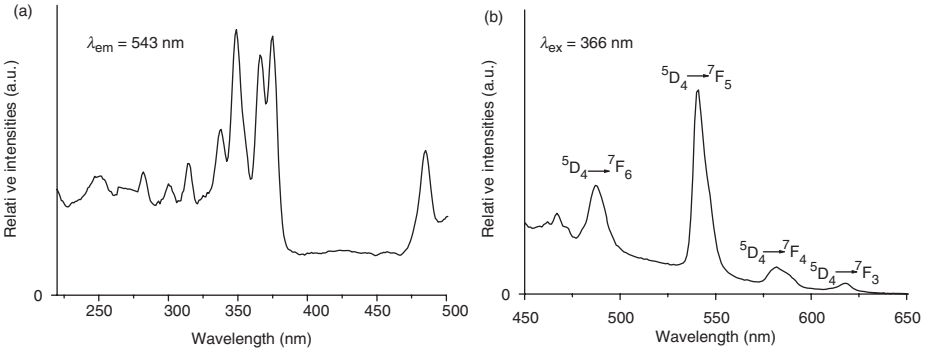

Figure 4. Excitation (a) and emission (b) spectra of $LaF_3:10\%Tb^{3+}$ nanoparticles.

be observed, which is due to the fact that the nano quantum effect forms the more extensive continuous energy distribution state. It seems possible that surface states generated from broken, truncated chemical bonds and the lack of long-range lattice order may be some possible cause(s) for this situation. For the slightly agglomerated nanoparticles, the existence of enormous surface states results in additional charge transfer transition and will provide energy to the ^5D_J states of Eu^{3+} to enhance the energy transfer to 7FJ states of Eu^{3+} [26]. Besides, there exist some narrow excitation bands in the long wavelength ultraviolet region to visible region, which corresponds to the 4f–4f transitions of Eu^{3+}. Among the electronic dipole transition $^7F_0 \rightarrow {}^5L_6$ shows the strongest excitation intensity, while the magnetic dipole transitions, $^7F_1 \rightarrow {}^5D_2$ and $^7F_0 \rightarrow {}^5D_1$, present the weakest intensity. Under the excitation of 394 nm, the $LaF_3:10\%$ Eu^{3+} nanoparticles exhibit the characteristic orange–red luminescence of Eu^{3+}, corresponding to the $^5D_0 \rightarrow {}^7F_J$ ($J = 0$–3) (Figure 3(b)). But the orange emission for $^5D_0 \rightarrow {}^7F_1$ transition (590 nm) shows the strongest intensity, which is stronger than that of red emission for $^5D_0 \rightarrow {}^7F_2$ transition (611, 616 nm). The orange–red emission lines at around 590 nm originating from the magnetic dipole transition $^5D_0$–$^7F_1$ are the dominant bands for $LaF_3:Eu^{3+}$, indicating that the Eu^{3+} occupied the inversion symmetry site [27]. It is well known that if Eu^{3+} occupies in the crystal lattice a site with inversion symmetry, the magnetic – dipole transitions $^5D_0 \rightarrow {}^7F_1$ of Eu^{3+} are dominant, and if there is no inversion symmetry at the site of Eu^{3+}, the main emission is the electric – dipole transition $^5D_0 \rightarrow {}^7F_2$. Besides this, both $^5D_0$–$^7F_1$ and $^5D_0$–$^7F_2$ transitions have splits by the crystal field, so that it can be observed that each transition splits into several components in the emission spectrum of $LaF_3:Eu^{3+}$ phosphors, which is in good agreement with the optical transitions observed in bulk $LaF_3:Eu^{3+}$.

Figure 4(a) gives the excitation spectra of $LaF_3:10\%Tb^{3+}$ nanoparticles, which are obtained by monitoring the $^5D_4$ – $^7F_5$ transition of Tb^{3+} ions at 541 nm. It can be clearly shown that the excitation spectra consist of two parts, one broad band in the 240–380 nm region, resulting from the well-known $^2F_{5/2}$ – 5d (or 4f–5d) transition of La^{3+}, and several sharp peaks in the 320–500 nm region related to the f–f transitions of Tb^{3+} ions. Figure 4(b) shows the emission spectrum of the obtained sample under excitation of 366 nm. The sharp emission peaks originate from the 4f–4f transition of Tb^{3+} ions : $^5D_4$–$^7F_6$ (488 nm), $^5D_4$–$^7F_5$ (541 nm), $^5D_4$–$^7F_4$ (582 nm) and very weak $^5D_4$–$^7F_3$ (618 nm).

4. Conclusions

In summary, the synthesis of $LaF_3:Eu^{3+}/Tb^{3+}$ nanoparticles has been achieved by a novel mixed-solvents-thermal (DMF/DFG) technology. Both XRD and TEM images present the pure hexagonal phase and homogeneous microstructure with particle size of 10 nm dimension. Under long broad ultraviolet excitation, red and green luminescence of Eu^{3+} and Tb^{3+} ion can be observed which indicates that it is a candidate technology for the synthesis of rare earth fluoride nanoparticles.

Acknowledgements

The work was supported by the Science Fund of Shanghai University for Excellent Youth Scientists and National Natural Science Foundation of China (20671072).

References

[1] J. Hu, Y. Bando, J. Zhan, and D. Golberg, *Growth of wurtzite ZnS micrometer-sized diskettes and nanoribbon arrays with improved luminescence*, Adv. Funct. Mater. 15 (2005), pp. 757–762.
[2] J.S. Steckel, J.P. Zimmer, and S. Coe-Sullivan, *Blue luminescence from (CdS)ZnS core-shell nanocrystals*, Angew. Chem. Int. Ed. 43 (2004), pp. 2154–2158.
[3] M. Han, Z. Gao, J.Z. Su, and S. Nie, *Quantum-dot-tagged microbeads for multiplexed optical coding of biomolecules*, Nat. Biotechnol. 19 (2001), pp. 631–637.
[4] A. Mayer and S. Neuenhofer, *Luminescent labels - more than just an alternative to radioisotopes*, Angew. Chem. Int. Ed. 33 (1994), pp. 1044–1047.
[5] A. Kikuchi, K. Yamano, and M. Tada, *Stimulated emission from GaN nanocolumns*, Phys. Stat. Sol. B 241 (2004), pp. 2754–2758.
[6] X.L. Gou, F.Y. Cheng, Y.H. Shi, L. Zhang, S.J. Peng, J. Chen, and P.W. Shen, *Shape-controlled synthesis of ternary chalcogenide $ZnIn_2S_4$ and $CuIn(S,Se)_2$ nano-/microstructures via facile solution route*, J. Am. Chem. Soc. 128 (2006), pp. 7222–7229.
[7] G.J. Zhou, M.K. Lu, Z.L. Xiu, S.F. Wang, H.P. Zhang, Y.Y. Zhou, and S.M. Wang, *Controlled synthesis of high-quality PbS star-shaped dendrites, multipods, truncated nanocubes, and nanocubes and their shape evolution process*, J. Phys. Chem. B 110 (2006), pp. 6543–6548.
[8] F.Y. Cheng, J.Z. Zhao, W.E. Song, C.S. Li, H. Ma, J. Chen, and P.W. Shen, *Facile controlled synthesis of MnO_2 nanostructures of novel shapes and their application in batteries*, Inorg. Chem. 45 (2006), pp. 2038–2044.
[9] C.M. Ho, J.C. Yu, T.Y. Kwong, A.C. Mak, and S.Y. Lai, *Morphology-controllable synthesis of mesoporous CeO2 nano- and microstructures*, Chem. Mater. 17 (2005), pp. 4514–4522.
[10] Z.Y. Wang, Z.B. Zhao, and J.S. Qiu, *Carbon nanotube templated synthesis of CeF_3 nanowires*, Chem. Mater. 19 (2007), pp. 3364–3366.
[11] L. Qu, L. Dai, and E.J. Osawa, *Shape/size-controlled syntheses of metal nanoparticles for site-selective modification of carbon nanotubes*, J. Am. Chem. Soc. 128 (2006), pp. 5523–5532.
[12] Q. Tang, W.J. Zhou, W. Zhang, S.M. Ou, K. Jiang, W.C. Yu, and Y.T. Qian, *Size-controllable growth of single crystal $In(OH)_3$ and In_2O_3 nanocubes*, Cryst. Growth Des. 5 (2005), pp. 147–150.
[13] W.C.W. Chan and S. Nile, *Quantum dot bioconjugates for ultrasensitive nonisotopic detection*, Science 281 (1998), pp. 2016–2018.
[14] H.M. Huang, J.N. Anker, K.M. Wang, and R. Kopelman, *Magnetically assisted and accelerated self-assembly of strawberry-like nano/microparticles*, J. Phys. Chem. B 110 (2006), pp. 19929–19934.

[15] Z.A. Peng and X.G. Peng, *Nearly monodisperse and shape-controlled CdSe nanocrystals via alternative routes: nucleation and growth*, J. Am. Chem. Soc. 124 (2002), pp. 3343–3353.
[16] L.T. Yu, I.A. Banerjee, and H. Matsui, *Direct growth of shape-controlled nanocrystals on nanotubes via biological recognition*, J. Am. Chem. Soc. 125 (2003), pp. 14837–14840.
[17] R.L. Penn and J.F. Banfield, *Imperfect oriented attachment: dislocation generation in defect-free nanocrystals*, Science 281 (1998), pp. 969–971.
[18] W. Sun, J.E. Puzas, T.J. Sheu, X. Liu, and P.M. Fauchet, *Nano- to microscale porous silicon as a cell interface for bone-tissue engineering*, Adv. Mater. 19 (2007), pp. 921–924.
[19] M.M. Lezhnina, T. Justel, H. Katker, D.U. Wiechert, and U.H. Kynast, *Efficient luminescence from rare-earth fluoride nanoparticles with optically functional shells*, Adv. Funct. Mater. 16 (2006), pp. 935–942.
[20] X. Wang, J. Zhuang, Q. Peng, and Y.D. Li, *Hydrothermal synthesis of rare-earth fluoride nanocrystals*, Inorg. Chem. 45 (2006), pp. 6661–6665.
[21] L. Zhu, Q. Li, X.D. Liu, J.Y. Li, Y.F. Zhang, J. Meng, and X.Q. Cao, *Morphological control and luminescent properties of CeF_3 nanocrystals*, J. Phys. Chem. C 111 (2007), pp. 5898–5903.
[22] Z.L. Wang, Z.W. Quan, P.Y. Jia, C.K. Lin, Y. Luo, Y. Chen, J. Fang, W. Zhou, C.J. O'Connor, and J. Lin, *Facile synthesis and photoluminescent properties of redispersible CeF_3, CeF_3: Tb^{3+}, and CeF_3: Tb^{3+}/LaF_3 (core/shell) nanoparticles*, Chem. Mater. 18 (2006), pp. 2030–2037.
[23] H. Lian, M. Zhang, J. Liu, Z.R. Ye, J. Yan, and C.S. Shi, *Synthesis and spectral properties of lutetium-doped CeF_3 nanoparticles*, Chem. Phys. Lett. 395 (2004), pp. 362–365.
[24] H. Zhang, H.F. Li, D.Q. Li, and S.L. Meng, *Synthesis and characterization of ultrafine CeF_3 nanoparticles modified by catanionic surfactant via a reverse micelles route*, J. Colloid Interface Sci. 302 (2006), pp. 509–515.
[25] S.Q. Qiu, J.X. Dong, and G.X. Chen, *Synthesis of CeF_3 nanoparticles from water-in-oil microemulsions*, Powder Technol. 113 (2000), pp. 9–15.
[26] J. Thirumalai, R. Chandramohan, M. Sekar, and R. Rajachandrasekar, *Eu^{3+} doped yttrium oxysulfide quantum structures-structural, optical and electronic properties*, J. Nanopart. Res. 10 (2008), pp. 455–463.
[27] G. Blasse and B.C. Grabmaier, *Luminescence Materials*, Springer-Verlag, Berlin, Germany, 1994.